Title: Dielectric properties of BiFeO3 ceramics obtained from mechanochemically synthesized nanopowders

Author: E. Markiewicz, B. Hilczer, M. Błaszyk, A. Pietraszko, Ewa Talik

Citation style: Markiewicz E., Hilczer B., Błaszyk M., Pietraszko A., Talik Ewa. (2011). Dielectric properties of BiFeO 3 ceramics obtained from mechanochemically synthesized nanopowders. "Journal of Electroceramics" (Vol. 27, no. 3/4 (2011), s. 154-161), DOI: 10.1007/s10832-011-9660-9

J Electroceram (2011) 27:154–161
DOI 10.1007/s10832-011-9660-9

Dielectric properties of $BiFeO_3$ ceramics obtained from mechanochemically synthesized nanopowders

E. Markiewicz · B. Hilczer · M. Błaszyk · A. Pietraszko · E. Talik

Received: 19 April 2011 / Accepted: 27 October 2011 / Published online: 9 November 2011

Abstract Dielectric behaviour of $BiFeO_3$ ceramics, obtained by hot-pressing of nanopowders produced by mechanochemical synthesis from Bi_2O_3 and Fe_2O_3 oxides (weight ratio 2:1), was studied in the temperature range 125–575 K. The ceramics was found to exhibit step-like dielectric response $\varepsilon^*(T)$ with high permittivity values, similar to the behaviour of materials with giant dielectric permittivity. Three overlapping relaxation processes contribute to the dielectric response: i) relaxation in the low-temperature range (220–420 K), characterized by activation energy of 0.4 eV, ii) relaxation in the temperature range 320–520 K with activation energy of 1.0 eV and iii) broad dielectric anomaly in the vicinity of 420 K, which disappears after 1 h annealing at 775 K. The low-temperature relaxation is ascribed to the carrier hopping process between Fe^{2+} and Fe^{3+} ions. The presence of mixed valence of the Fe ions was proved by X-ray photoelectron spectroscopy. Dielectric relaxation in the middle-temperature range is considered as a result of grain boundary effect and internal barrier layers related to $Bi_{25}FeO_{40}$ phase as verified by X-ray diffraction. The high-temperature dielectric anomaly we relate to short-range hopping of ordered oxygen vacancies.

Keywords $BiFeO_3$ · Powders-solid state reaction · Defects · Dielectric properties · Electrical conductivity

E. Markiewicz (✉) · B. Hilczer · M. Błaszyk
Institute of Molecular Physics, Polish Academy of Sciences,
M. Smoluchowskiego 17,
60-179 Poznań, Poland
e-mail: ewamar@ifmpan.poznan.pl

A. Pietraszko
Institute of Low Temperatures and Structure Research,
Polish Academy of Sciences,
Okólna 2,
50-422 Wrocław, Poland

E. Talik
August Chełkowski Institute of Physics, University of Silesia,
Uniwersytecka 4,
40-007 Katowice, Poland

1 Introduction

The interest in materials with high dielectric permittivity value is still increasing due to their wide applications in microelectronics industries. Among so called giant permittivity compounds with room temperature permittivity $\varepsilon' \sim 10^5$ the most important are $ACu_3Ti_4O_{12}$ [1, 2] and complex perovskites $AFe_{1/2}B_{1/2}O_3$ [3]. It is widely proposed in the literature that the unusual dielectric behavior of the materials is related to the electrically inhomogeneous microstructure (grain-boundary structure) of the ceramics that enhances the dielectric permittivity by the barrier layer mechanism [4–10]. Malone and Subramanian point out to the contribution of electric conductivity originating from the multivalent Cu and Fe ions and oxygen vacancies [11]. It appears that the problem of electric conductivity in $BiFeO_3$ (BFO), which is the most studied single phase room temperature magnetoelectric multiferroic, is of great importance because the temperature at which the antiferromagnetic ordering disappears (T_N=640 K) is significantly removed from the ferroelectric Curie temperature (T_C=1100 K) [12].

Recently the magnetoelectric multiferroics gain a great interest because the magnetoelectric (ME) coupling opens up an opportunity to design and develop advanced magnetoelectric RAMs, magnetic field sensors, spintronics elements etc. [13–18]. It has been shown however that the ME coupling is not the only way to induce high magneto-dielectric response but the response may originate from

various kinds of heterogeneity as grain boundary layers and superlattices [19]. Kamba et al. have shown that the magnetodielectric response of BFO ceramics in the temperature range 10–300 K is not originating from the ME effect (coupling of dielectric polarization and magnetization in the multiferroic) but is due to a combination of Maxwell-Wagner type polarization and the magnetoresistance [20]. They found that the relative changes in the dielectric permittivity under influence of magnetic field up to 9 T at the temperature above 250 and bellow 200 K, i. e., in the range where the Maxwell—Wagner mechanism does not contribute to the permittivity, are very low ($\sim 10^{-5}$).

It should however be noted that the dielectric response and electric conductivity of BFO ceramics are determined by the processing conditions [21–25], which are responsible not only for the oxygen deficiency and the presence of Fe^{2+} but also for the formation of various parasitic phases [26, 27]. BFO ceramics obtained by rapid liquid phase sintering [21, 22] as well as ceramics sintered from coprecipitation powder at 800°C and 850°C [23] are single-phased ceramics of a high electric resistivity with ferric Fe^{3+} ions. Low ac conductivity of BFO ceramics sintered from powders obtained in coprecipitation process was measured at low temperatures (at 25°C: $\sim 2 \cdot 10^{-5}$ Ω^{-1} m^{-1} and $\sim 2 \cdot 10^{-4}$ Ω^{-1} m^{-1} for 100 kHz and 2 MHz, respectively) with activation energy of 0.13 eV. At temperatures higher than ~350°C the conductivity increases rapidly with activation energy of 1.26 eV and its low-frequency values become higher than those for the high frequency [23]. Another dielectric behaviour with three relaxation processes have been reported for the ceramics sintered at 700°C during 4 h from pure precipitation-synthesized BFO powder [25]. The low-temperature relaxation with activation energy of 0.34 eV was attributed by the authors to the hopping conductivity of the localized charge carriers, the middle-temperature relaxation process of the activation energy 0.77 eV was related to the grain boundary effect, whereas the high-temperature relaxation with the highest activation energy (0.95 eV) to the defects and/or the conduction.

Hence, it appears that a fundamental understanding of the correlations between the structure and the properties in BFO ceramics is still inadequate. To improve the understanding of the problem we report here the results of the dielectric response studies of hot-pressed ceramics obtained by hot-pressing of BFO nanopowders prepared by a mechanochemical synthesis (solid-solid reaction initiated by milling in high-energy ball mills). The parameters of the mechanochemical process, like milling time, shock frequency and the kinetic energy per hit, strongly affects the properties of the milling product, as well as the value of the dielectric permittivity [28]. We discover that the obtained ceramics exhibits a high dielectric permittivity. It has been established that three dielectric relaxation processes contribute to the dielectric response in the temperature range 125–575 K. X-ray diffraction (XRD) analysis reveal the presence of a trace of $Bi_{25}FeO_{40}$ and we understand that the parasitic phase plays an important role in the observed dielectric properties. The electrical inhomogeneity of the material enables us to justify the relatively giant value of dielectric permittivity using the well–known *internal barrier layer capacitor model* [4, 5, 8]. In addition, X-ray photoelectron spectroscopy (XPS) studies were performed in order to evaluate the contents of mixed valences Fe^{2+} and Fe^{3+} ions, since the perovskites containing polyvalent cations such as Fe, Mn and Cu are known to exhibit a prominent dielectric permittivity step due to electron transfer between both valence states [6, 11, 29].

2 Experimental

2.1 Sample preparation

Bismuth ferrite nanopowder was synthesized by high-energy mechanical activation of commercially available oxides Bi_2O_3 (99.8% purity) and Fe_2O_3 (99% purity) purchased from Aldrich. The starting oxides weighted in $2Bi_2O_3$:Fe_2O_3 ratio were placed in 250 ml stainless steel vial and subjected to high-energy milling using 10 grinding balls of 20 mm diameter made of stainless steel too. The weight ratio of the balls to the powder was 30:1. The mechanochemical synthesis was performed in Fritsch Pulverisette 6 planetary ball mill during 7 h under normal pressure. The calculated parameters [30] of the high energy milling were the following: the kinetic energy per hit and the shock frequency were 300 mJ/hit and 100 Hz, respectively. The obtained nanopowder was hot-pressed at 1073 K under pressure of 200 MPa during 2 h using graphite die/ram tool in order to compact the ceramics. Typical dimensions of samples were ~8 mm diameter and ca. 1 mm thickness. Both sides of the samples subjected to dielectric measurements were coated with gold electrodes using Baltec SCD 050 sputter coater.

2.2 XRD studies

The structure of the synthesized BFO was controlled by X-ray powder diffraction studies using X'Pert-PANalytical diffractometer with CuKα radiation. The data were collected at room temperature in 2–theta range from 10° to 60° after milling and after the hot–pressing process of the sample.

2.3 XPS measurements

XPS spectra of BFO ceramic sample were recorded using a PHI 5700/660 Physical Electronics Photoelectron

Spectrometer with monochromatized Al K_α X-ray radiation (1,486.6 eV). The Fe *2p* core level XPS spectra of BFO ceramic samples were collected with UHV (standard pressure of 8×10^{-11} mBar) VG Scienta spectrometer with SES 100 analyzer. Measurements were performed with Mg anode (1,254 eV) at room temperature. In addition, in order to refine the samples surfaces, ion beam etching was carried out preceding each measurement. In every case the binding energy was determined by reference to the C*1s* component at the energy of 285 eV.

2.4 Dielectric measurements

Dielectric response and ac conductivity of the BFO ceramic samples were studied using an Alpha-A High Performance Frequency Analyzer (Novocontrol GmbH) combined with Quatro Cryosystem for the temperature control. The sample was fixed between two additional external electrodes in the sample holder and placed into a cryostat. The measurement was performed in the temperature range from 125 K to 575 K on heating at a rate of 1 K/min. The frequency varied from 1 Hz to 1 MHz at the oscillation voltage of 1 V. The measured dielectric permittivity data were collected and evaluated by WinDETA impedance analysis software and a WinFit V 3.2. program.

3 Results and discussion

X-ray powder diffraction studies revealed the structure of the synthesized BFO as trigonal (R3*c*). The mean grain size calculated according to the Scherer formula [31], was 26 nm after milling and 64 nm after hot–pressing. Figure 1 shows the XRD patterns of BFO nanopowder after milling and that after hot–pressing. The spectrum observed for the nanopowder immediately after milling shows the presence of X-ray diffraction peak at *2Θ* angle of about 27.2° considered as belonging to pure Bi. The trace of Bi disappears after hot-pressing at 1073 K due to both the high volatility of this element and formation of a parasitic phase. The spectrum recorded after the hot-pressing is characterized by a number of diffraction peaks at about 27.7°, 54.0° and 55.6° owing to the contribution of secondary $Bi_{25}FeO_{40}$ phase. The peak of relatively high intensity in the vicinity of 44.2° is coming from the iron sample holder. Moreover, a weak diffraction peak of unknown origin was observed at 46.7°. We assigned the positions of particular X-ray diffraction peaks to the components using ISCD 2010 data base of inorganic compounds.

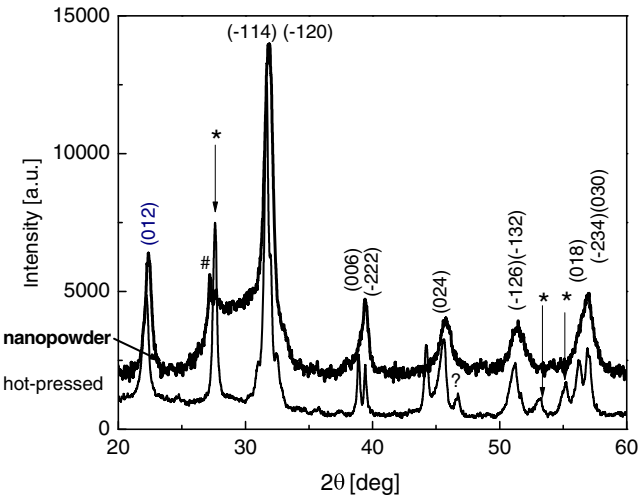

Fig. 1 XRD patterns of BFO nanopowder obtained by high energy ball milling (the upper line) and after hot-pressing (the bottom line); the line marked by # is attributed to metallic Bi, the lines marked by stars with arrows are ascribed to $Bi_{25}FeO_{40}$

As both the presence of a parasitic phase and the mixed valence of iron ions are very crucial to the dielectric properties of the ceramics, BFO was also characterized by XPS spectroscopy. Figure 2 shows XPS spectrum of the ceramics obtained from mechanically synthesized nanopowders by hot-pressing. One can observe that the characteristic core level spectra manifest themselves at the energies higher than ~20 eV and the valence band is separated from the Fermi level by energy gap of ~2.2 eV (see the inset). Fe *2p* core level XPS spectrum of the BFO ceramics obtained from mechanochemically synthesized nanopowders is presented in Fig. 3. The line shape deconvolution of the Fe $2p_{3/2}$ maximum (Gaussian-Lorentzian curve fitting) yields two peaks which can be ascribed to the presence of both Fe^{3+} and Fe^{2+} ions with binding energies of 709.4 eV and 707.8 eV, respectively [32]. The integrated intensities of the two contributions are comparable (that of the Fe^{2+} $2p_{3/2}$ is of ~51% of the total Fe $2p_{3/2}$ component, that of Fe^{3+} $2p_{3/2}$ is of ~49% of the

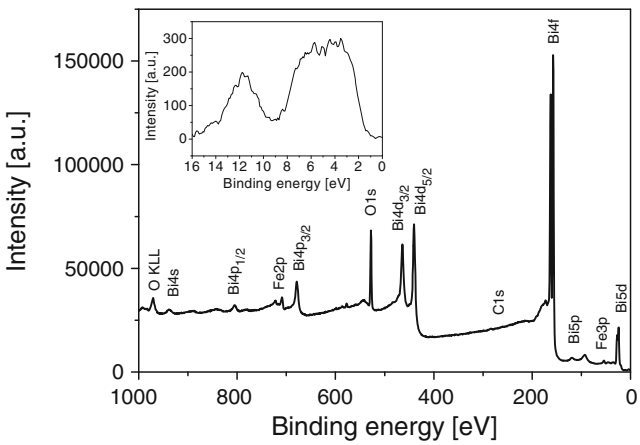

Fig. 2 XPS spectrum of the ceramics obtained from mechanically synthesized powders by hot-pressing

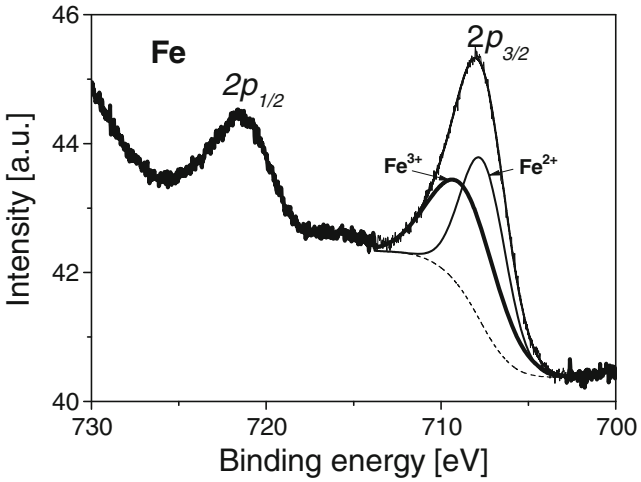

Fig. 3 Fe *2p* core level XPS spectrum of the BFO ceramics obtained from mechanochemically synthesized powders

total Fe $2p_{3/2}$ maximum) which implies ~50% of the iron ions occurring in the Fe^{2+} valence state. The composition of the BFO ceramics was calculated from the integrals of "Bi4*f*", "Fe2*p*" and "O1*s*", the three photoelectron profiles, with the following sensitivity correction factors: Bi—31 at.%, Fe—10.5 at.% and O—58.5 at.%. Thus determined composition differs considerably from the $BiFeO_3$ stoichiometry and is due to the ratio of the oxides used for mechanochemical synthesis ($2Bi_2O_3$:Fe_2O_3). The Bi surplus is apparent in the hot-pressed ceramics as well as the admixture of bismuth-rich $Bi_{25}FeO_{40}$ phase observable in the XRD pattern.

Figure 4 shows temperature dependences of real ε' and imaginary ε'' parts of dielectric permittivity of the hot-pressed BFO sample. Only below 150 K one can observe the intrinsic permittivity of $\varepsilon' \approx 80$. At higher temperatures the two parts of dielectric permittivity remarkably rise due to the contribution of three dielectric relaxation processes that occur in the temperature ranges: 220–370 K, 350–470 K and in the vicinity of 420 K. Following the nomenclature of Hunpratub *et al.* [25], we denote the three temperature ranges as the *low–temperature dielectric relaxation* (LTDR), *middle–temperature dielectric relaxation* (MTDR) and *high–temperature dielectric relaxation* (HTDR), respectively. A step-like decrease in the ε' value between successive relaxation processes is characteristic of so—called giant dielectric constant materials as Ba$(Fe_{1/2}Nb_{1/2})O_3$, Sr$(Fe_{1/2}Nb_{1/2})O_3$ [33] and $CaCu_3Ti_4O_{12}$ [34]. Both the low—and middle—temperature dielectric relaxations are characterized by a strong dispersion. On rising the frequency the maxima of dielectric absorption of both LTDR and HTDR shift towards higher temperatures, whereas the maximum related to the HTDR only weakly depends on the temperature.

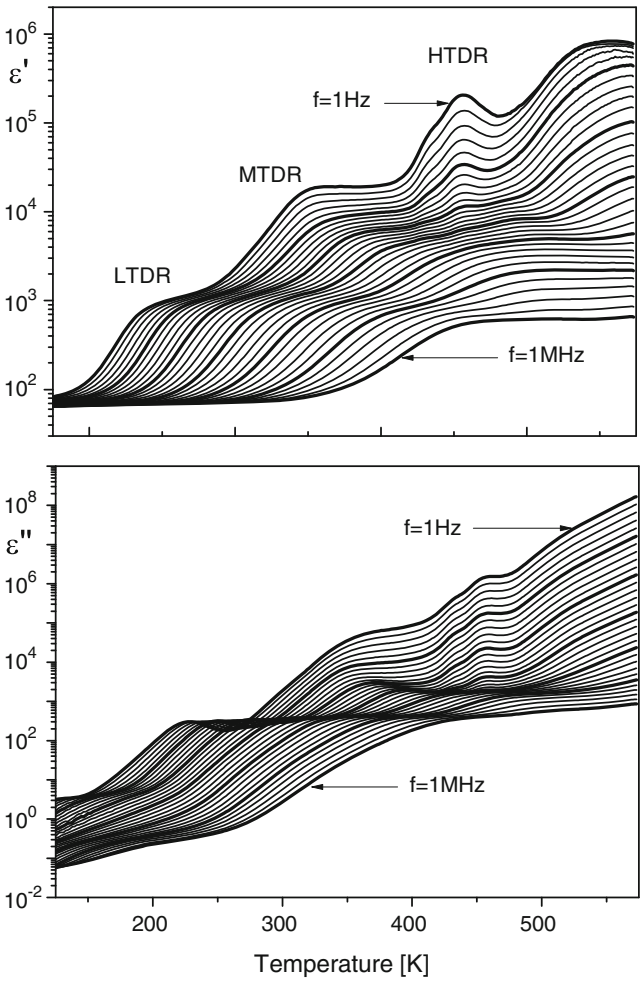

Fig. 4 Temperature dependences of real ε' and imaginary ε'' parts of dielectric permittivity of the hot–pressed BFO sample

To understand the physical nature of LTDR and MTDR, the experimental results of dielectric spectrum measurement were fitted to the Cole—Cole equation superposed to the conductivity term [35]:

$$\varepsilon(\omega) = \varepsilon' - i\varepsilon'' = -i\left(\frac{\sigma_0}{\varepsilon_0\omega}\right)^N + \sum_{k=1}^{2}\left[\frac{\Delta\varepsilon_k}{1+(i\omega\tau_k)^{\alpha}} + \varepsilon_{\infty k}\right], \quad (1)$$

where: k denotes the number of relaxation processes, Δ—difference between the permittivity value at the lowest at highest frequency of the dispersion step, ε_∞—the permittivity value at the highest frequency, ε_0—the dielectric constant of free space, α—degree of the distribution of relaxation times τ, σ_0—the specific dc conductivity, N—exponent of the frequency dependence of ε''. Figure 5 shows the frequency dependences of ε'' at four temperatures in the range of LTDR and MTDR processes. The experimental data (the squares) are in a good agreement with the best fits to the Cole—Cole equation, represented

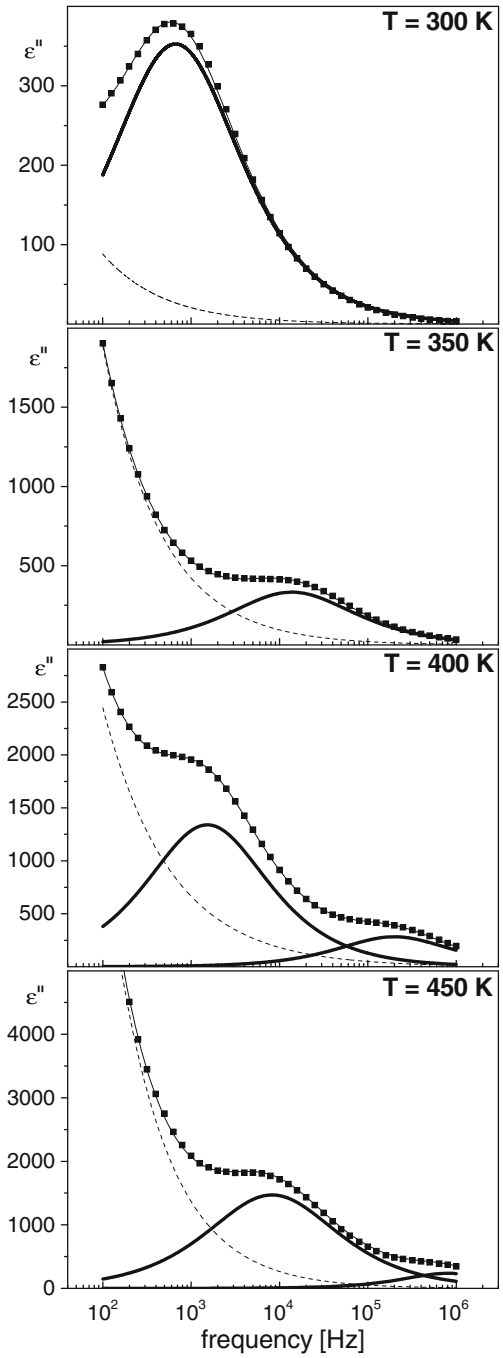

Fig. 5 Frequency dependences of imaginary part ε'' of dielectric permittivity at four temperatures in the range of LTDR and MTDR processes

by the continuous lines drawn over the points. The dashed line is related to the conductivity term $\left(\frac{\sigma_0}{\varepsilon_0\omega}\right)^N$ in the Eq. 1. The other continuous lines refer to the contributions of separated relaxation processes. It is clearly seen from the fitting results that both LTDR and MTDR are of the Debye-type. The values of α were obtained to be 0.74–0.79 for the LTDR and 0.83–0.95 for the MTDR. Based on the fitting results, it can be verified that the relaxation times of both LTDR and MTDR obey the Arrhenius law:

$$\tau(T) = \tau_0 \exp(E_a/k_B T), \tag{2}$$

where τ_0 denotes the preexponential factor, E_a is the activation energy required for relaxation process, and k_B is the Boltzmann constant. Figure 6 shows the relaxation times of the both processes plotted as a function of reciprocal temperature. The activation energy E_a values calculated from Eq. 2 are: 0.39 and 0.98 eV for the LTDR and MTDR, respectively. The relatively small energy of the low-temperature relaxation is characteristic of the process originated from the ordering of Fe^{2+} and Fe^{3+} in the arrangement of polar symmetry [36]. Two-site polaron hopping process of the charge transfer between Fe^{2+} and Fe^{3+} leads to the hopping conduction of the localized charge carrier inside the grain. The obtained E_a value (0.4 eV) compares well with 0.325 eV for $BiFeO_3$ ceramics prepared from pure precipitation-synthesized powder [25], 0.21 eV for $YFeO_3$ [29] and 0.29 eV for $LuFe_2O_4$ [36]. The mutual feature of the LTDR in these ceramics leads us to suppose that the LTDR process in BFO ceramics obtained from mechanochemically synthesized nanopowders is related to mixed valence of the iron ions. This mixed-valence ferrous/ferric structure was confirmed in the XPS experiments (Fig. 3). The ordering of the cations with mixed valence can produce polar clusters that grow in size with decreasing temperature but do not freeze, hence the thermally activated dielectric relaxation process is possible. The larger the number of dipoles the larger the magnitude of the dielectric permittivity ε' step. For instance, the ratio of Fe^{2+}:Fe^{3+} in $Sr(Fe_{1/2}Nb_{1/2})O_3$ amounts to 1:1, which yields 10^3 dielectric permittivity step [33], whilst the relatively small fraction of Fe^{2+}:Fe^{3+} in $YFeO_3$, namely 1:4 is the reason for the permittivity step of the order of just ten [29]. The BFO ceramics prepared from mechanochemically obtained powders, with almost the same contents of

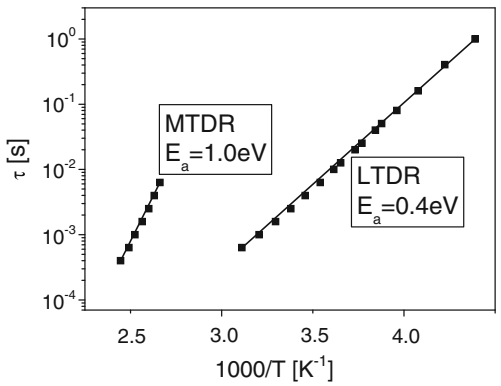

Fig. 6 Relaxation times of the both LTDR and MTDR processes plotted as a function of reciprocal temperature

Fe^{2+} and Fe^{3+} cations shows the dielectric permittivity ε' step of about 10^3.

The behavior of MTDR seems very similar to that reported for so-called giant dielectric constant materials and is closely related to the microstructure, in particular, to the grain boundary, grain sizes and defect structure [21–27]. Shao *et al.* reported the relationship between the microstructures and activation energies of the MTDR of $CaCu_3Ti_4O_{12}$ ceramics [37] and an enhancement of the relaxation due to presence of parasitic phase [38]. Sinclair *et al.* demonstrated that $CaCu_3Ti_4O_{12}$ ceramics is electrically inhomogeneous and consists of semiconducting grains with insulating grain boundaries and related the giant dielectric phenomenon to a grain boundary (internal) barrier layer capacitor [39, 40]. The grain boundary effect was also observed in the ceramics obtained from pure precipitation-synthesized $BiFeO_3$ powder: the samples synthesized at 973 K were characterized by a pronounced grain and grain boundary configuration and exhibited strong MTDR with activation energy of 0.69 eV [25]. In the case of our BFO ceramics obtained from mechanochemically synthesized nanopowders, the MTDR can be attributed to the combined effect of the grain boundary and the presence of secondary $Bi_{25}FeO_{40}$ phase acting as an additional internal barrier layer making the heterogeneity more complex. The secondary phase can be considered as a semiconducting one due to its energy gap of 1.78 eV [41]. The activation energy of 1.0 eV is slightly higher compared to that of BFO obtained from pure precipitation-synthesized powder, probably due to the increase in the heterogeneity. Although the authors suspect that the MTDR can be attributed to the combined effect originating from the grain boundaries and the secondary $Bi_{25}FeO_{40}$ phase, the electron microscopy investigations should be undertaken to confirm this assumption. The microscopic grain boundary studies will be the subject of our future study.

In order to study the physical nature of HTDR, we measured the frequency dependence of ac conductivity (σ_{ac}) in the temperature range from 400 K to 570 K at 10 K

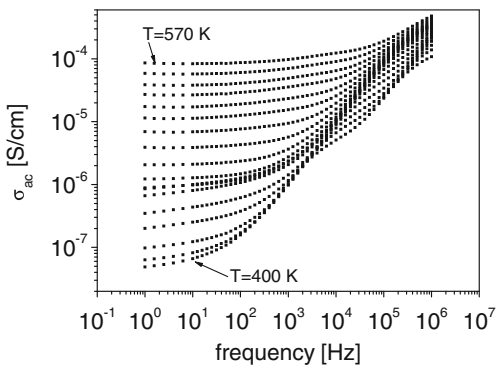

Fig. 7 Frequency dependence of σ_{ac} of hot-pressed BFO sample at several temperatures between 400 and 570 K

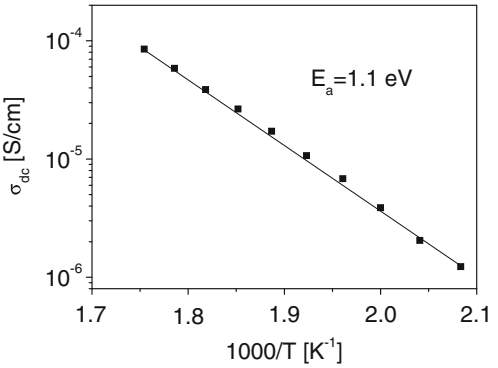

Fig. 8 σ_{dc} of hot-pressed sample as the function of reciprocal temperature

steps and we compared the dielectric spectra for the hot-pressed sample and the sample annealed in the air at 775 K for 1 h. Figure 7 shows the frequency dependence of σ_{ac} at several temperatures. The σ_{ac} indicates a dispersion which shifts towards higher frequencies with increasing the temperature. At low frequencies, the conductivity σ_{ac} saturates to a constant value i.e. the dc conductivity σ_{dc}. The resulting σ_{dc} is plotted as the function of reciprocal temperature in Fig. 8. In the plot one can see, it properly obeys the Arrhenius law:

$$\sigma_{dc} = \sigma_0 \exp(E_a/k_B T), \tag{3}$$

where σ_0 is the pre-exponential term. The calculated value of activation energy E_a=1.1 eV is very near to 1.08 eV

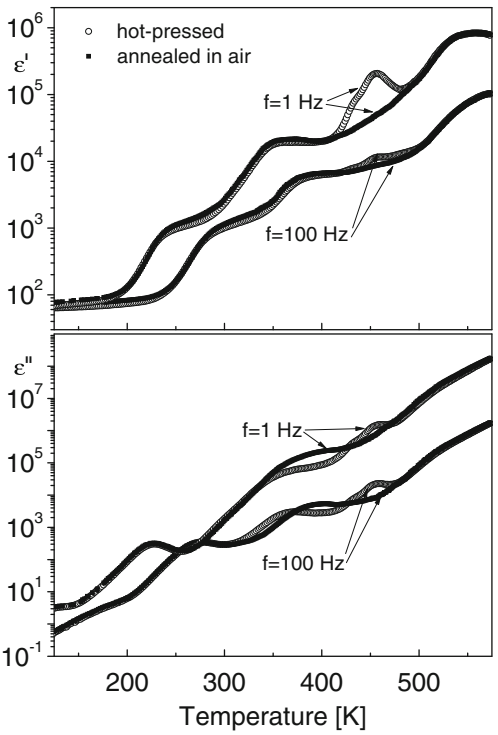

Fig. 9 Influence of annealing at 775 K in air on the real ε' and imaginary ε'' parts of dielectric permittivity

obtained for $YFeO_3$ in the high temperature range (469–579 K) [29] and 0.99–1.12 eV for $(Sr_{1-1.5x}Bi_x)TiO_3$ ($0.0133 \leq x \leq 0.133$), also at higher temperatures (550–680 K) [42]. The values of activation energy are typical for doubly ionized oxygen vacancies $V_0^{''}$. It was reported by Waser *et al.* [43] that the oxygen vacancies in Bi doped $SrTiO_3$ can move due to the thermal activation. The mobility of oxygen vacancy at 513 K can attain $7 \cdot 10^{-9}$ $cm^2/(Vs)$ and the activation energy of oxygen vacancy is 1.093 eV. Moreover, Paladino [44] did prove that the activation energy for the diffusion of the doubly—ionized oxygen vacancies in $SrTiO_3$ crystal is 0.98 eV. Based on these results, we suggest that, the HTDR process is related to the oxygen vacancies $V_0^{''}$ commonly present in perovskite structures. A short-range hopping of the oxygen vacancies resembles the dipolar reorientation and results in a dielectric relaxation peak, whereas long-range motion of double-ionized oxygen vacancies leads to the dc conductivity. One should also presume that other point defects may contribute into HTDR.

The influence of annealing at 775 K in air on the real ε' and imaginary ε'' parts of dielectric permittivity is shown in Fig. 9. The temperature of the annealing was chosen based on our previous DSC measurement results which revealed the exothermic oxygen sorption process in the vicinity of 775 K, similarly like in other perovskite-type oxides [45]. Moreover, the chosen temperature is low enough to prevent the volatilization of Bi. The annealing was performed for the samples with evaporated gold electrodes as well as without them. The dielectric measurement results allow us to state that the electrodes do not change the composition of the annealed samples. It appears that the LTDR behavior is almost unaffected by the annealing process, though a small temperature range extension of the permittivity step of the MTDR is observed. The annealing process was found however, to smear out the HTDR: the two ε' and ε'' maxima disappear. Considering that the dielectric permittivity ε' steps of both LTDR and MTDR rise after annealing due to suppression the HTDR peaks, we can argue that the dielectric steps in the dielectric spectrum of the BFO ceramics result from a competition balance of the relaxation processes. The dielectric permittivity ε' steps of both LTDR and MTDR lengthen after annealing. The above results are quite similar to those reported earlier in $Ba(Fe_{1/2}Nb_{1/2})O_3$ [46] $Ba(Fe_{1/2}Ta_{1/2})O_3$ [33] and $YFeO_3$ [29].

4 Conclusions

BFO ceramic with addition of $Bi_{25}FeO_{40}$ secondary phase was obtained from nanopowders produced by high energy ball milling of Bi_3O_3 and Fe_2O_3 oxides of the weight ratio 2:1. The obtained BFO ceramics can be considered as a material of high dielectric permittivity that is very promising from the application point of view. Three dielectric relaxation processes in the low—(LTDR) middle—(MTDR) and high (HTDR) temperature range were found to contribute to the dielectric response. The LTDR, characterized by the activation energy of 0.4 eV, is related to hopping of electronic charge carriers, which are produced to compensate the changes in the oxidation state of iron ions. This argument is supported by the mixed-valence Fe^{2+}/Fe^{3+} structure evidenced in the Fe $2p_{3/2}$ core level XPS spectra. The MTDR, with activation energy of 1.0 eV, is considered as originating from a contribution of grain boundaries and the secondary $Bi_{25}FeO_{40}$ phase acting as an internal barrier layers. The HTDR, which can be suppressed by thermal annealing, may be related to short-range hopping of the ordered oxygen vacancies. Long-range transport of double-ionized oxygen vacancies results in dc conductivity, which reaches 10^{-6} S/cm and $8.5 \cdot 10^{-5}$ S/cm at 480 K and 570 K, respectively and is characterized by an activation energy of 1.1 eV. As the dielectric permittivity steps are results of the competing balance of the three relaxation processes, it seems to be very probable that dielectric response may be tailored to the application requirements by optimizing the parameters of the mechanochemical synthesis and thermal treatment.

Acknowledgement The work was supported by the funds from European Concerted Research Action designated as COST Action MP0904: Single- and multiphase ferroics and multiferroics with restricted geometries (SIMUFER).

References

1. A.P. Ramirez, M.A. Subramanian, M. Gardela, G. Blumberg, D. Li, T. Vogt, S.M. Shapiro, Giant dielectric constant response in a copper-titanate. Solid State Commun. **115**, 217–220 (2000)
2. M.A. Subramanian, D. Li, N. Duan, B.A. Reisner, A.W. Sleight, High dielectric constant in $ACu_3Ti_4O_{12}$ and $ACu_3Ti_3FeO_{12}$ phases. J. Solid State Chem. **151**, 323–325 (2000)
3. I.P. Raevski, S.A. Prosandeev, A.S. Bogatin, M.A. Malitskaya, L. Jastrabik, High dielectric permittivity in $AFe_{1/2}B_{1/2}O_3$ nonferroelectric perovskite ceramics (A=Ba, Sr, Ca;B=Nb, Ta, Sb). J. Appl. Phys. **93**, 4130–4136 (2003)
4. M.H. Cohen, J.B. Neato, L. He, D. Vanderbilt, Extrinsic models for the dielectric response of $CaCu_3Ti_4O_{12}$. J. Appl. Phys. **94**, 3299–3306 (2003)
5. G. Cao, L. Feng, C. Wang, Grain-boundary and subgrain-boundary effects on the dielectric properties of $CaCu_3Ti_4O_{12}$ ceramics. J. Phys. D Appl. Phys. **40**, 2899–2905 (2007)
6. C. Wang, H.J. Zhang, P.M. He, G.H. Cao, Ti-rich and Cu-poor grain-boundary layers of $CaCu_3Ti_4O_{12}$ detected by x-ray photoelectron spectroscopy. Appl. Phys. Lett. **91**, 052910-1-3 (2007)

7. C.C. Wang, L.W. Zhang, Anomalous thermal hysteresis in dielectric permittivity of $CaCu_3Ti_4O_{12}$. Appl. Phys. Lett. **92**, 132903-1-3 (2008)
8. P. Fiorenza, R. Lo Nigro, C. Bongiorno, V. Raineri, M.C. Ferarrelli, D.C. Sinclair , A.R. West, Localized electrical characterization of the giant permittivity effect in $CaCu_3Ti4O_{12}$ ceramics. Appl. Phys. Lett. **92**, 182907-1-3 (2008)
9. D. Fu, H. Taniguchi, T. Taniyama, M. Itoh, S. Koshihara, Origin of giant dielectric response in nonferroelectric $CaCu_3Ti_4O_{12}$: inhomogeneous conduction nature probed by atomic force microscopy. Chem. Mater. **20**, 1694–1698 (2008)
10. S.Y. Chung, Comment on "Origin of giant dielectric response in nonferroelectric $CaCu_3Ti_4O_{12}$: inhomogeneous conduction nature probed by atomic force microscopy". Chem. Mater. **20**, 6284–6285 (2008)
11. M. Maglione, M.A. Subramanian, Dielectric and polarization experiments in high loss dielectrics: a word of caution. Appl. Phys. Lett. **93**, 032902-1-3 (2008)
12. G. Catalan, J.F. Scott, Physics and applications of bismuth ferrite. Adv. Mater. **21**, 2463–2485 (2009)
13. Ch Binek, B. Doudin, Magnetoelectronics with magnetoelectrics. J. Phys. Condens. Matter. **17**, L39–L44 (2005)
14. M. Bibes, A. Barthélémy, Toward a magnetoelectric memory. Nat Mater. **7**, 425–426 (2008)
15. Y.-H. Chu, L.W. Martin, M.B. Holcomb, M. Gajek, S.-J. Han, Q. He, N. Balke, C.-H. Yang, D. Lee, W. Hu, Q. Zhan, P.-L. Yang, A. Fraile-Rodríguez, A. Scholl, S.X. Wang, R. Ramesh, Electric-field control of local ferromagnetism using a magnetoelectric multiferroic. Nat Mater. **7**, 478–482 (2008)
16. C-M Lin, W. Shih, I.Y. Chang, P-C Juan, J.Y. Lee, Metal-ferroelectric ($BiFeO_3$)-insulator (Y_2O_3)-semiconductor capacitors and field effect transistors for nonvolatile memory applications. Appl. Phys. Lett. **94**, 142905-1-3 (2009)
17. Z. Xing, J. Zhai, J. Li, D. Viehland, Investigation of external noise and its rejection in magnetoelectric sensor design. J. Appl. Phys. **106**, 024512-1-7 (2009)
18. P. Rovillain, R. de Sousa, Y. Gallais, A. Sacuto, M.A. Méasson, D. Colson, A. Forget, M. Bibes, A. Barthélémy, M. Cazayous, Electric-field control of spin waves at room temperature in multiferroic $BiFeO_3$. Nat Mater. **9**, 975–979 (2010)
19. G. Catalan, Magnetocapacitance without magnetoelectric coupling. Appl. Phys. Lett. **88**, 102902-1-3 (2006)
20. S. Kamba, D. Nuzhnyy, M. Savinov, J. Šebek, J. Prokleška, R. Daumont, J. Kreisel, Infrared and terahertz studies of polar phonons and magnetodielectric effect in multiferroic $BiFeO_3$ ceramics. Phys. Rev., B **75**, 024403-1-7 (2007)
21. Y.P. Wang, L. Zhou, M.F. Zhang, X.Y. Chen, J.-M. Liu, Z.G. Liu, Room-temperature saturated ferroelectric polarization in $BiFeO_3$ ceramics synthesized by rapid liquid phase sintering. Appl. Phys. Lett. **84**, 1731–1733 (2004)
22. A.K. Pradhan, K. Zhang, D. Hunter, J.B. Dadson, G.B. Loutts, P. Bhattacharya, R. Katiyar, J. Zhang, D.J. Sellmyer, U.N. Roy, Y. Cui, A. Burger, Magnetic and electrical properties of single-phase multiferroic $BiFeO_3$. J. Appl. Phys. **97**, 093903-1-4 (2005)
23. J-C Chen, J-M Wu, Dielectric properties and ac conductivities of dense single-phased $BiFeO_3$ ceramics. Appl. Phys. Lett. **91**, 182903-1-3 (2007)
24. S.V. Selbach, T. Tybel, M.-A. Einarsrud, T. Grande, The ferroic phase transitions of $BiFeO_3$. Adv. Mater. **20**, 3692–3696 (2008)
25. S. Hunpratub, P. Thongbai, T. Yamwong, R. Yimnirun, S. Maensiri, Dielectric relaxations and dielectric response in multiferroic $BiFeO_3$ ceramics. Appl. Phys. Lett. **94**, 062904-1-3 (2009)
26. M. Valant, A.-K. Axelsson, N. Alford, Peculiarities of a solid-state synthesis of multiferroic polycrystalline $BiFeO_3$. Chem. Mater. **19**, 5431–5436 (2007)
27. Y.U. Jian, C.J. Hao, Progress and prospect for high temperature single-phased magnetic ferroelectrics. Chin. Sci. Bull. **53**, 2097–2112 (2008)
28. L.B. Kong, T.S. Zhang, J. Ma, F. Boey, Progress in synthesis of ferroelectric ceramic materials via high-energy mechanochemical technique. Progress Mater. Sci. **53**, 207–322 (2008)
29. Y. Ma, X.M. Chen, Y.Q. Lin, Relaxorlike dielectric behavior and weak ferromagnetism in $YFeO_3$ ceramics. J. Appl. Phys. **103**, 124111-1-5 (2008)
30. M. Abdellaoui, E. Gaffet, The physics of mechanical alloying in a planetary ball mill: mathematical treatment. Acta Metall. Mater. **43**, 1087–1098 (1995)
31. R. Jenkins, R.L. Snyder, *Introduction to X-ray Powder Diffractometry.* (John Wiley & Sons Inc., 1996)
32. J. Chastain, R.C. King Jr. (eds.), *Handbook of X–ray Photoelectron Spectroscopy* (Physical Electronics Inc., Minnesota, 1992)
33. Y.Y. Liu, X.M. Chen, X.Q. Liu, L. Li, Giant dielectric response and relaxor behaviors induced by charge and defect ordering in $Sr(Fe_{1/2}Nb_{1/2})O_3$ ceramics. Appl. Phys. Lett. **90**, 192905-1-3 (2007)
34. L. Ni, X.M. Chen, Dielectric relaxations and formation mechanism of giant dielectric constant step in $CaCu_3Ti_4O_{12}$ ceramics. Appl. Phys. Lett. **91**, 122905-1-3 (2007)
35. A.K. Jonscher, *Dielectric relaxation in solids* (Chelsea Dielectrics Press Ltd, London, 1983)
36. N. Ikeda, H. Ohsumi, K. Ohwada, K. Ishii, T. Inami, K. Kakurai, Y. Murakami, K. Yoshii, S. Mori, Y. Horibe, H. Kito, Ferroelectricity from iron valence ordering in the charge-frustrated system $LuFe_2O_4$. Nature **436**, 1136–1138 (2005)
37. S.F. Shao, J.L. Zhang, P. Zheng, W.L. Zhong, C.L. Wang, Microstructure and electrical properties of $CaCu_3Ti_4O_{12}$ ceramics. J. Appl. Phys. **99**, 084106-1-11 (2006)
38. S.F. Shao, J.L. Zhang, P. Zheng, C.L. Wang, J.C. Li, M.L. Zhao, High permittivity and low dielectric loss in ceramics with the nominal compositions of $CaCu_{3-x}La_{2x/3}Ti_4O_{12.}$ Appl. Phys. Lett. **91**, 042905-1-3 (2007)
39. D.C. Sinclair, T.B. Adams, F.D. Morrison, A.R. West, $CaCu_{3-}Ti_4O_{12}$: One-step internal barrier layer capacitor. Appl. Phys. Lett. **80**, 2153–2155 (2002)
40. T.B. Adams, D.C. Sinclair, A.R. West, Giant barrier layer capacitance effects in $CaCu_3Ti_4O_{12}$ ceramics. Adv. Mater. **14**, 1321–1323 (2002)
41. G.-Q. Tan, Y.-Q. Zheng, H.-Y. Miao, A. Xia, H.-J. Ren, Controllable microwave hydrothermal synthesis of bismuth ferrites and photocatalytic characterization. J. Am. Ceram. Soc. **94**, 1–10 (2011)
42. C. Ang, Z. Yu, L.E. Cross, Oxygen-vacancy-related low-frequency dielectric relaxation and electrical conduction in Bi: $SrTiO_3$. Phys. Rev. B **62**, 228–236 (2000)
43. R. Waser, T. Baiatu, K.H. Hrdtl, Dc Electrical Degradation of Perovskite–Type Titanates: I, Ceramics. J. Am. Ceram. Soc. **73**, 1645–1653 (1990)
44. A.E. Paladino, Oxydation Kinetics of Single Crystal $SrTiO_3$. J. Am. Ceram. Soc. **48**, 476–478 (1965)
45. Z.H. Yang, Y.S. Lin, Synergetic thermal effects for oxygen sorption and order-disorder transition on perovskite-type oxides. Solid State Ionics **176**, 89–96 (2005)
46. Z. Wang, X.M. Chen, L. Ni, YY Liu, X.Q. Liu, Dielectric relaxations in $Ba(Fe_{1/2}\ Ta_{1/2})O_3$ giant dielectric constant ceramics. Appl. Phys. Lett. **90**, 102905-1-3 (2007)